JOURNAL OF AIRCRAFT
Vol. 47, No. 4, July–August 2010

# Propeller Empennage Interaction Effects on Vertical Tail Design of Multiengine Aircraft

M. J. T. Schroijen,* L. L. M. Veldhuis,† and R. Slingerland‡
*Delft University of Technology, 2629 HS Delft, The Netherlands*

DOI: 10.2514/1.46707

**A potential-flow model for conceptual design and vertical tail sizing purposes, currently under development, has been applied and tested in an investigation of the influence of the propeller slipstream on the empennage flowfield. Additionally, the model is intended to increase the understanding of the phenomena arising in propeller–empennage interaction. For verification purposes and complementation to limited wind-tunnel results in open literature, dedicated measurements were performed and supplemented by a Reynolds-averaged Navier–Stokes analysis. From wind-tunnel measurements, in one-engine-inoperative condition, it is found that the empennage experiences a propeller-induced crossflowfield, which is found to be the main contributor to the additional yawing moment experienced by the measured multiengine propeller aircraft. The most probable cause for deviation in yawing moments in measurements and the potential-flow model is incorrect modeling of the flowfield behind the wing. This was verified by a comparison of the measured and computed flowfield behind the wing and in front of the vertical tail. Efforts to create a potential model to aid in conceptual vertical tail sizing should, therefore, focus on achieving realistic wing-wake behavior. In this respect, the effect of the propeller on the wing-lift distribution, as well as the wing-wake aircraft interaction, should be treated with care.**

## Nomenclature

| | | |
|---|---|---|
| $b$ | = | wing span, m |
| $C_D$ | = | drag coefficient |
| $C_n$ | = | yawing moment coefficient |
| $C_{n_s}$ | = | static yawing moment coefficient, $(2Ty_p)/(S_{\text{ref}}\rho V_\infty^2 b)$ |
| $C_T$ | = | thrust coefficient, $2T/(S_{\text{ref}}\rho V_\infty^2)$ |
| $c$ | = | wing chord, m |
| $c_l$ | = | local lift coefficient |
| $E$ | = | ratio between flap and total wing chord, $c_f/(c_f + c_w)$ |
| $F$ | = | side force, n |
| $f$ | = | propeller rotation frequency, Hz |
| $J$ | = | advance ratio |
| $P$ | = | pressure, N/m$^2$ |
| $S$ | = | surface area, m$^2$ |
| $T$ | = | thrust, N |
| $T_c$ | = | thrust coefficient, $2T/(S_p\rho V_\infty^2)$ |
| $v_t$ | = | tangential flow velocity, m/s |
| $y_P$ | = | propeller location in $y$ direction, m |
| $\alpha$ | = | angle of attack, deg |
| $\beta$ | = | sideslip angle, deg |

*Subscripts*

| | | |
|---|---|---|
| $D$ | = | dorsal fin |
| $F$ | = | fuselage |
| $f$ | = | flap |
| $i$ | = | installed |
| $P$ | = | propeller |
| $T$ | = | tail |
| $t$ | = | total |
| $u$ | = | uninstalled |
| $W$ | = | wing |
| $\beta$ | = | derivative with respect to sideslip angle |

Received 12 August 2009; revision received 24 February 2010; accepted for publication 6 March 2010. 

*Ph.D. Student, Faculty of Aerospace Engineering, Systems Engineering and Aircraft Design; M.J.T.Schroijen@TUDelft.nl.

†Associate Professor, Faculty of Aerospace Engineering, Aerodynamics and Wind Energy; L.L.M.Veldhuis@TUDelft.nl.

‡Assistant Professor, deceased (26 October 2007).

## I. Introduction

THE traditional use of statistical methods in the conceptual design of multiengine propeller aircraft has resulted in considerable safety factors and possible overdimensioning of the vertical tail, due to limited understanding of the effects driving the design. This overdimensioning results in an increase in drag and, subsequently, a decrease in transport efficiency. However, increasing the efficiency by reducing the overdimensioning can only be achieved if current safety standards are met. A better understanding of the effects driving the horizontal and vertical tail is therefore essential. Conceptual design of multiengine propeller aircraft has been complicated by the interaction between the propeller slipstream and aircraft. Torenbeek [1] notes that with respect to propeller aircraft "the yawing and rolling moments induced by engine failure present control problems and downgrade the flight performance, in particular when the engine fails in the takeoff." Raymer [2] also notes that "wing mounting of engines introduces engine-out controllability problems that force an increase in the size of the rudder and vertical tail." Vertical tailplane design is determined by stability and controllability considerations, especially in one-engine-inoperative (OEI) conditions during takeoff. A significant contribution to the stability and controllability considerations is posed by the propeller–empennage interaction, by means of the propeller slipstream [3]. Research on this interaction has focused on obtaining relations between propeller settings and resulting stability derivatives with limited attention to the physics underlying this interaction.

Mannée [3], in an early research, showed that there is a significant contribution to the yawing moment of an aircraft, in OEI condition, due to the interaction of propeller slipstream and vertical tail. Stuper [4] had already identified that the wing significantly alters the propeller slipstream. To quantify this effect, he performed measurements in the wake of a jet–wing and a propeller–wing combination. More recent experimental research by Veldhuis [5], Gamble and Reeder [6], and Roosenboom et al. [7] has been carried out to quantify the deformation of the flowfield behind the propeller and wing due to their interaction.

Further research on the propeller–tail interaction has focused on effects on either longitudinal or directional stability. Eshelby [8] modeled the effect of the propeller–wing–tail interaction on the

longitudinal stability by means of a potential-flow model. This model was, however, limited to the effect of the propeller's induced axial velocity and the altered wing-lift distribution on the horizontal tail. Katzoff [9] has conducted experiments using various aircraft to determine the longitudinal stability, using the propeller thrust coefficient as a variable. More recently, Qin et al. [10] coupled a propeller vortex panel method with an aircraft vortex panel method obtaining aircraft longitudinal forces and moments. Van Rooyen and Eshelby [11] performed measurements to determine the thrust effects of multiple propellers on the stability coefficients of a twin-engine aircraft.

The relation between the vertical tail design and the propeller–tail interaction, which may have considerable impact on directional stability, has received limited attention in open literature. The primary objective in this article is to provide a method which is based on flow physics rather than empirical relations. Furthermore it is to be used in the conceptual design phase of multiengine propeller aircraft. This method should be able to model the interactions (e.g., propeller–wing and propeller–vertical tail). To create such a model, an understanding for the underlying phenomena is needed.

## II. Method

As a starting point for the sizing of the vertical tail, the condition of equilibrium state after engine loss was used [1]. The yawing moment induced by the propeller in OEI condition has to be balanced by the vertical tail, including rudder. To be able to determine the size of the vertical tail the aerodynamic directional forces and moments in OEI condition have to be determined. The air flow around the aircraft in this flight phase is generally complex:

1) The aircraft is flying at an angle of sideslip resulting in nonsymmetrical flow around the fuselage and wing.

2) The aircraft is usually in a high lift condition that results in nonlinear aerodynamic effects (low speed and high thrust) and limited controllability.

3) The flow is distorted due to the inoperative engine, resulting in additional drag, especially if the propeller is not feathered.

This complex flow pattern is shown schematically in Fig. 1. To reduce the complexity of the model, while still incorporating all dominant effects, several assumptions are used:

1) The sideslip angle is set to zero, resulting in the inability to fulfill the steady condition in OEI.

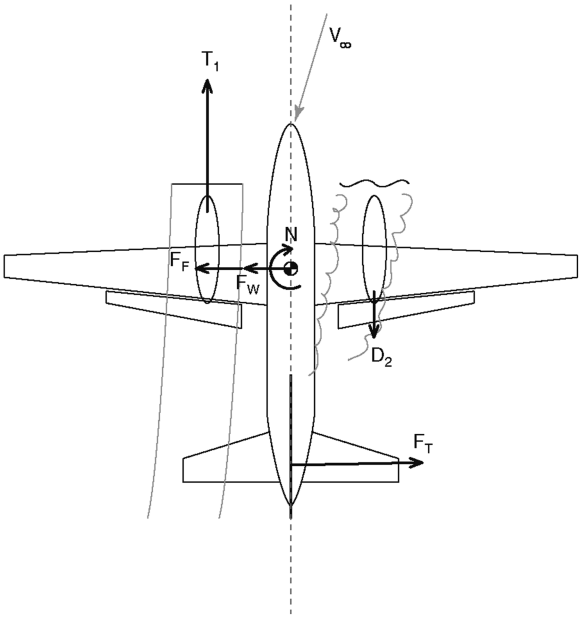


**Fig. 1 General situation of a twin-engine aircraft with starboard engine inoperative. Included are the most important forces and moments acting on the aircraft components.**

2) The feathering state of the inoperative propeller is simulated by removal of the propeller, which means that the additional drag is assumed to be negligible.

3) The aircraft is assumed to operate in the linear region of the lift curve.

4) The horizontal tail is not included, which decreases the stabilizing effect of the empennage on the aircraft's yawing moment [12,13].

5) The aircraft has two engines, for this configuration the propeller-induced destabilizing effects in OEI condition are assumed to be dominant.

With these simplifications an aerodynamic model based on potential flow was created. This model was able to calculate the directional forces and moments. The results from the computational model were compared with wind-tunnel measurements, both dedicated measurements and from literature, and a Reynolds-averaged Navier–Stokes (RANS) model.

### A. Potential-Flow Model

The numerical aerodynamic model is based on potential methods and is described more extensively in previous work [14,15]. The propeller is modeled by vortex theory [16] with a correction for the finite number of blades [17]. The wing, flap and vertical tail, without dorsal fin, are modeled by Prandtl's lifting line theory, including the interaction with the fuselage [18–20]. The deformation of the wing trailing vortex sheet (WTVS) is computed by a fourth-order Runge–Kutta time stepping method [21,22]. Since potential models have numerical difficulties due to the singularities used to model the flow, two situations have been considered, a WTVS which was prescribed and without roll up (nondeformed) and the time stepping method, where the vortex sheet was allowed to roll up (deformed). In both situations the propeller slipstream boundary was assumed to be a rigid cylinder.

The input consists of basic aircraft geometric and control parameters, employed during conceptual design, propeller geometric and control parameters, and flight condition parameters. The geometry modelling is shown schematically in Fig. 2. The output gives the yawing moment and side force coefficient of the components and the complete configuration.

### B. Measurements

Three types of measurements in OEI condition were performed in the low speed, low turbulence wind tunnel at the Delft University of Technology. First, forces and moments were measured to determine the power-on effects on the complete configuration. Second, sidewash was measured in front of the vertical tail to determine whether this could provide a sufficient explanation for the additional side force and yawing moment. Finally, velocity vectors were determined behind the inboard wing, to capture the path of the inboard flap tip vortex and part of the propeller slipstream for a better understanding of the flowfield behind the wing, inboard of the nacelle.

#### *1. Wind-Tunnel Model Description*

The wind-tunnel model was a 1:20 scale two-engine Fokker F27 model ($b_W = 1.45$ m, $l_F = 1.155$ m), with double-slotted inboard and outboard flaps and a removable horizontal tail Fig. 3. The horizontal tail plane was removed for two reasons: to be able to measure in the flowfield behind the wing and to reduce complexity by removing the interference effects as it has a stabilizing effect on the directional control [12,13]. The two engines present to drive the two constant pitch propellers ($D_P = 0.183$ m) were high-frequency three-phase induction motors rated at 3.6 kW. In the measurements, only one of these engines was fitted with a propeller to simulate the OEI condition. Both port and starboard engines were used for inboard (IU) and outboard up (OU) measurements, resulting in four situations, as will be explained in more detail in Sec. II.B.3. The rotation directions are defined as given in Fig. 4.

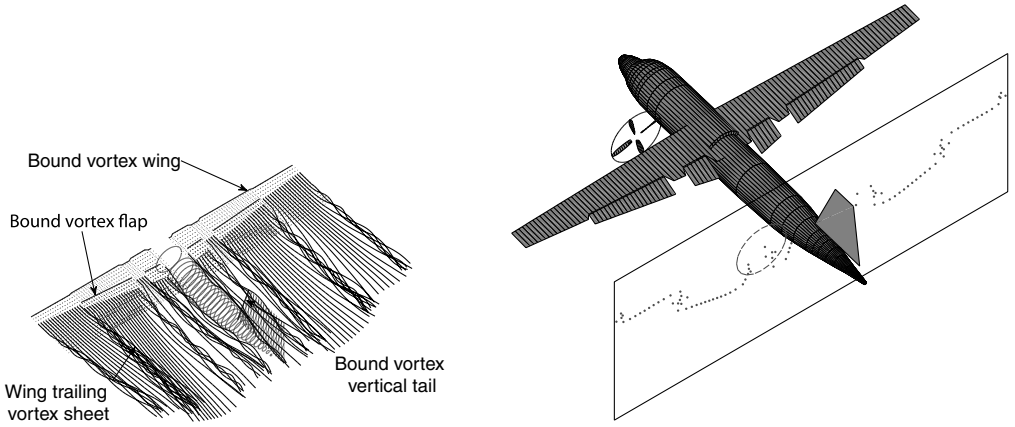


**a) Vortex distributions** **b) Representative geometry**

**Fig. 2 Fokker F27 geometry used in the potential-flow model.**

To obtain a thrust setting comparable to a go-around maneuver, the advance ratio ($\frac{V}{nD}$) was kept as low as possible. This was obtained by choosing the highest practical propeller revolution speed (280 Hz) combined with the lowest freestream velocity (40 m/s) that prevented serious Reynolds number effects. Moreover, the propeller speed was limited by engine cooling capacity. The resulting Reynolds number based on the wing chord of 350,000 was rather low and transition strips at 30% of the wing and fin chord were used to prevent laminar separation of the boundary layer.

The measurements were performed with the inboard and outboard flaps deflected over 24° at an angle of attack of 0° and 6° at a constant sideslip angle of 0°.

### 2. *Measurement Equipment*

The forces and moments were measured with the wind tunnel's external six-component balance system. The model was connected to this balance system by three struts, two mounted at the wings and one at the aft body (tail strut), as depicted in Figs. 3 and 5. The tail strut was used to control the angle of attack of the model and to feed power and coolant to the engines. The model was inverted to minimize the disturbances by the mountings as shown in Fig. 6. A conical head, five-hole probe [5], with a diameter of 1.65 mm, was used for the quantitative measurements in front of the vertical tail and behind the wing. It was calibrated in the range of −45 to 45° and positioned at 1.9° angle of attack and 11.9° angle of sideslip to reach all areas of interest. Moving the probe was done via an electronic traversing system.

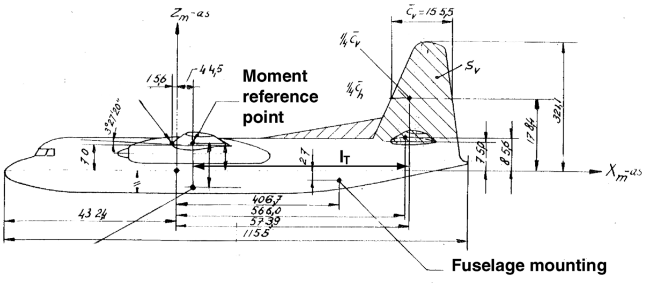


**Fig. 3 F27 model and mounting points, the moment point is also the wing mounting point adapted from Binkhorst [24].**

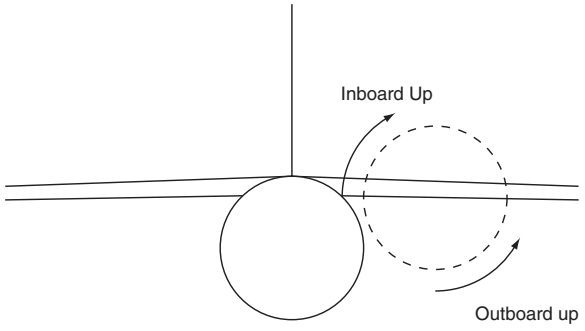


**Fig. 4 IU and OU propeller rotation direction (aircraft seen from the front).**

### 3. *Measurement Data Processing*

The balance measurements were corrected for wind-tunnel wall and support interference effects. Zero measurements were performed to determine the forces and moments without propellers installed. These were subtracted from the forces and moments with one propeller installed to determine the thrust coefficient:

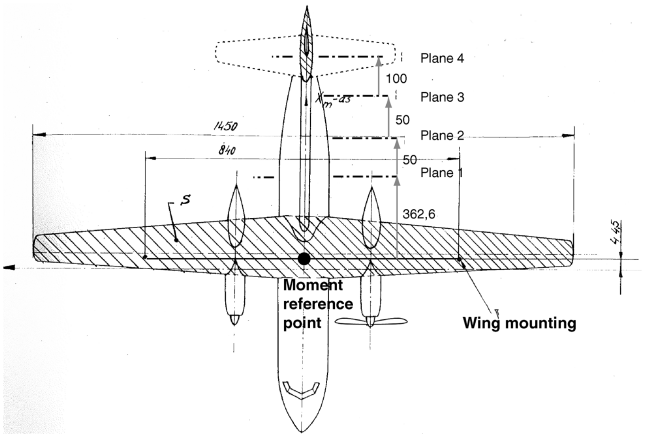


**Fig. 5 F27 model with mounting points, and the stations used for flow measurements behind the wing, adapted from Binkhorst [24].**

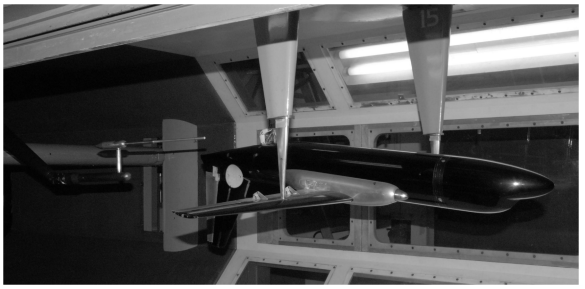

**Fig. 6 The F27 model as mounted belly up in the wind tunnel. In the back, the five-hole probe and traversing system can be seen.**

$$T_c = \frac{S_\infty}{S_P}[C_D(\alpha, \delta_f, J = 0) - C_D(\alpha, \delta_f, J)] \quad (1)$$

In this way, the net installed thrust coefficient was obtained. The zero installed power measurements were also used to correct for initial asymmetries in the model. The balance measurements were performed for both the starboard and port engine allowing for a correction of thrust effects on the model asymmetries, by a least squares approximation. The yawing moments are related to the static yawing moment ($C_{n_s}$), which is defined as the net thrust times the moment arm. Moreover, the yawing moment coefficient is defined by the difference in moment between the configuration without propeller and with running propeller.

The sidewash measurements were performed in the plane of symmetry in front of the vertical tail as indicated in Fig. 7, where the sidewash velocities should be zero when using a symmetrical model. The velocity vectors were, therefore, corrected for the slight asymmetries in the model and support system, by performing a measurement without propellers installed and subtracting these values from the propeller operative values.

The five-hole probe was mounted such that one side of the WTVS could be measured behind the propeller, wing and flap. To perform measurements on the opposite side of the operative engine, the propeller was uninstalled and installed on the opposite side instead of modifying the traversing system of the pitot probe. The measured velocities were calculated in the body frame of reference. To determine the vorticity strength a central difference scheme was used.

### C. Reynold-Averaged Navier–Stokes Model

To investigate further discrepancies between the measurements and numerical model, a computational model was made using the Fluent flow solver to model the configuration as measured by Mannée [3].

The propeller disc was modeled as an actuator disc with appropriate propeller-induced axial and tangential slipstream velocities. The input for the RANS propeller model (fan) was set to obtain the same installed thrust as used by Mannée [3], using the vortex theory model mentioned in Sec. II.A. The resulting values for the total pressure jump, $\Delta P_t$, and the induced tangential velocity component, $v_t(r)$, were used as input in the RANS fan model [23]. The configuration employed in the RANS model is shown in Fig. 8. The grid was unstructured with 1.7 million tetrahedral cells. Furthermore, the solver used was steady laminar and linear, with a semi-implicit method for pressure-linked equations coupling between pressure and momentum.

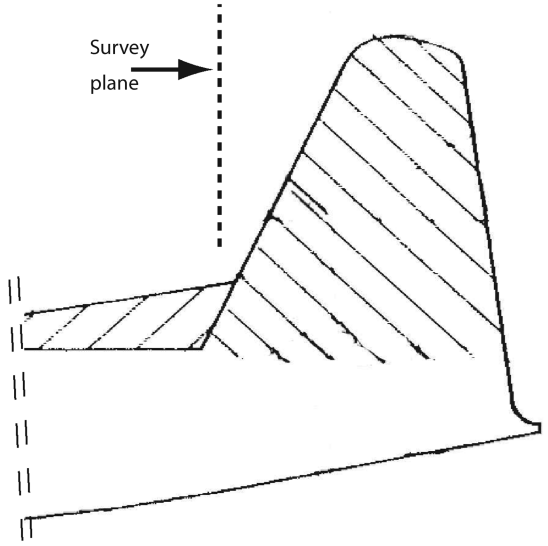


**Fig. 7 Location of the sidewash measurements in the plane of symmetry of the vertical tail.**

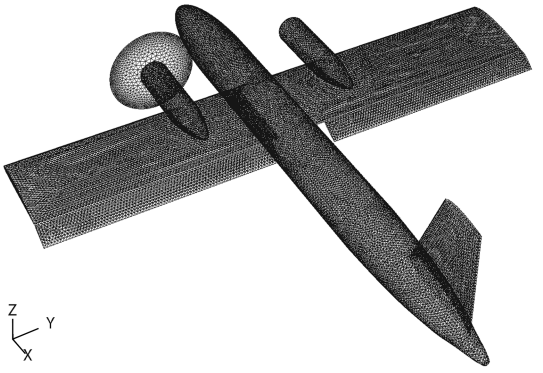


**Fig. 8 Schematic representation of the configuration as used in the RANS model and in the experiments by Mannée [3].**

## III. Results

The potential-flow model, described in Sec. II, is compared with the data obtained from the dedicated measurements and the work of Mannée [3]. To verify the potential-flow model the various contributions of the components separately, engineering sciences data unit (ESDU) methods as well as measurements performed by Binkhorst [24] are used in a flow with propellers inoperative.

### A. Comparison of the Yawing Moment

In Fig. 9 the measured yawing moment coefficient versus the thrust coefficient is depicted along with and their least squares approximations. The range of obtained thrust coefficients, from −0.1 to 0.6, is small in comparison with the ones employed by Mannée, 0.0 to 2.0, nevertheless, the relative increase in yawing moment is similar to that of larger thrust coefficients. This observation suggests that these measurements are representative and usable for validating the potential-flow model. When both measured and calculated yawing moment coefficients are compared, as visualized in Fig. 10, the calculated coefficients clearly show an underestimation. To evaluate the most important contribution to this yawing moment, the point of application of the additional side force is determined. Referring back to the measurements and assuming that all side forces operate in the same direction and have a point of application behind the moment reference point, the point of application of the additional side force can be determined by

$$\frac{l}{b} = -\frac{\Delta C_n}{\Delta C_y} = -\frac{\partial \Delta C_n}{\partial T_c}\frac{\partial T_c}{\partial \Delta C_y} \quad (2)$$

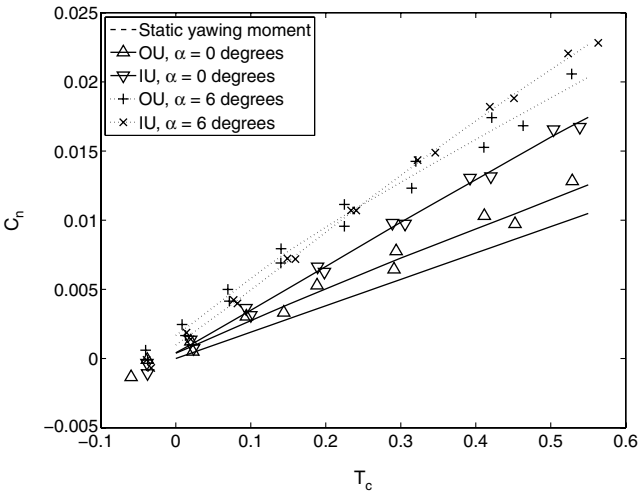


**Fig. 9 Measured thrust versus yawing moment curve for the Fokker F27 configuration with flaps deflected $\delta_f = 24°$ at $\alpha = 0$ and 6°.**

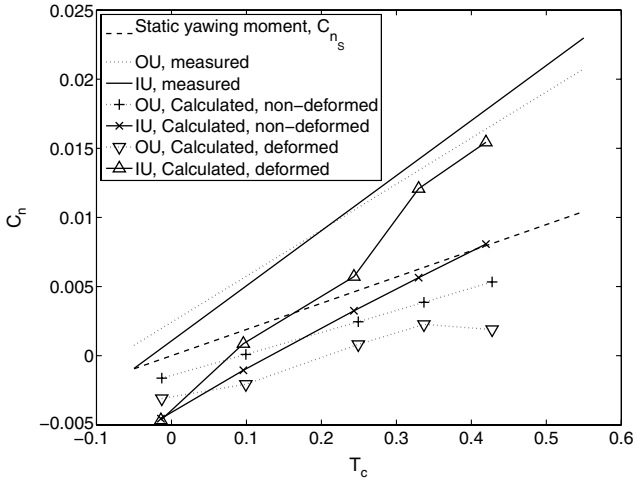


**Fig. 10 Yawing moment coefficient as measured and calculated with the potential model for the Fokker F27 configuration with flaps deflected $\delta_f = 24°$ at $\alpha = 6°$.**

Table 1, containing the nondimensional moment arms, suggests that the additional side force and yawing moment coefficient are caused by the vertical tail plane, with a moment arm of $\frac{l_T}{b} = 0.365$. Here $l_T$ is defined as given in Fig. 3, the distance between the moment point and the quarter chord position at the mean chord location of the vertical tail in the aircraft reference frame.

To verify the implication that the vertical is the main contributor to the additional yawing moment, the contributions of the aircraft components are investigated separately. The yawing moment coefficient contribution of each aircraft component (indexed $i$) is assumed to consist of an equivalent sideslip angle $(\bar{\beta})_i$ and a yawing moment coefficient derivative $(C_{n_\beta})_i$,

$$\Delta C_n = \sum_i (C_{n_\beta})_i (\bar{\beta})_i \tag{3}$$

The implicit assumption is made, that the effects of a variation in thrust, angle of attack, and propeller rotation direction can be represented as an equivalent sidewash at the component location. The yawing moment coefficient derivatives $(C_{n_\beta})_i$ are verified by placing the aircraft without propeller in a uniform flow at a finite angle of sideslip without thrust effects. The effects of the propeller on the aircraft are evaluated by comparing the measured and calculated sidewash in front of the vertical tail.

### B. Comparison of the Yawing Moment Derivative

Neglecting the propeller influence for the moment, the aircraft is split into two major components of which the yawing moment coefficient derivatives are determined: the wing fuselage and the vertical tail. The analysis is done in a uniform flow at a finite angle of sideslip and zero angle of attack, with flaps retracted. The measurements performed by Binkhorst [24] as well as ESDU methods [25,26] are used as references. The potential-flow model results for the yawing moment derivatives were obtained by putting the aircraft at a finite sideslip angle.

**Table 1 Averaged additional yawing moment coefficient and side force coefficient, and resulting moment arm**

| $\alpha$ | | $\frac{\partial C_n}{\partial T_c}$ | $\frac{\partial C_Y}{\partial T_c}$ | $\frac{l}{b}$ |
|---|---|---|---|---|
| 0° | IU | 0.0122 | −0.0422 | 0.289 |
| | OU | 0.0031 | −0.0095 | 0.326 |
| 6° | IU | 0.0211 | −0.0488 | 0.432 |
| | OU | 0.0149 | −0.0469 | 0.318 |

#### 1. Wing–Fuselage Contribution

The upper part of Table 2, index WF, shows that the yawing moment derivative of the potential model for the wing–fuselage combination agrees well with the measured and computed verification values. The side force derivative, however, is significantly underestimated, which is probably caused by neglecting viscous effects on the front and aft part of the fuselage [27]. Furthermore, the nacelle influence and the fact that the fuselage is approximated by a cylinder, equal in height to the actual fuselage, instead of the actual more elliptic shape are also a cause for errors in fuselage contribution [28]. Moreover, the compensating effect of the wing on the yawing moment derivative was found to be lower than indicated by House and Wallace [28]. Most sources for error are found to be determined by the contribution of the nose of the fuselage at an angle of yaw. The OEI measurements, however, have been performed using zero sideslip angle, in which case these sources of error do not occur and the model produces valid results for the contribution of the fuselage–wing combination.

According to van Rooyen and Eshelby [11] the contribution of the nacelles is negligible in OEI conditions. This is supported by the potential-flow model where the modeled nacelles seem to have a negligible contribution.

#### 2. Vertical Tail Contribution

The contribution of the vertical tail to the side force and yawing moment derivative is obtained by subtracting the values for wing and fuselage from the total side force and yawing moment derivatives. These values, therefore, include the additional contribution due to the fuselage–fin interaction. The results, shown in the lower part of Table 2, index $T$, indicate that the error for the yawing moment derivative is smaller than the ESDU method and well within the range of 10%, generally employed for conceptual design purposes.

The previous paragraphs show that the error found in yawing moment for the complete configuration with flaps deflected in OEI conditions is not caused by the modeling of the components in a uniform flowfield at a finite angle of sideslip. The cause for difference should, therefore, be sought in an error in calculated sidewash in the situation where the propeller is operating.

### C. Comparison of the Sideslip Angle

The second comparison, the sideslip angle, is performed by comparing the five-hole probe measurements to the calculated sidewash in front of the vertical tail plane. Figures 11a and 11b , showing the additional sidewash ($\Delta v_y$) due to thrust effects, show considerable differences in magnitude as well as trend. The calculated side force due to the vertical tail is consequently smaller as well as the resulting additional yawing moment. Further comparison of the calculated results, in particular including WTVS deformation, does not show the expected difference in sidewash expected from previous work, as shown in Fig. 12. Further investigation of the vortex sheet shape is therefore required. According to Mannée [3] this sidewash is caused by the asymmetrical wing-lift distribution. Two contributions are assumed: first, the sidewash due to the asymmetrical shape of the vortex field caused by the asymmetrical roll up of the sheet and second, an asymmetrical vortex strength distribution of the WTVS. Both effects are closely related and cannot be seen completely separated.

The first effect is closely related to the asymmetric movement of the flap tip inner vortex due to the WTVS and fuselage effect. Previous work [14,15] suggests that the position of the flap inner

**Table 2 Comparison of the directional stability derivatives, $\alpha = 0°$**

| | $(C_{n_\beta})_{WF}$ | $(C_{Y_\beta})_{WF}$ | $(C_{n_\beta})_T$ | $(C_{Y_\beta})_T$ |
|---|---|---|---|---|
| Binkhorst [24] | −0.073 | −0.1709 | 0.231 | −0.696 |
| ESDU [26] | −0.054 | −0.1679 | 0.289 | −0.794 |
| Potential model | −0.092 | −0.0736 | 0.233 | −0.629 |

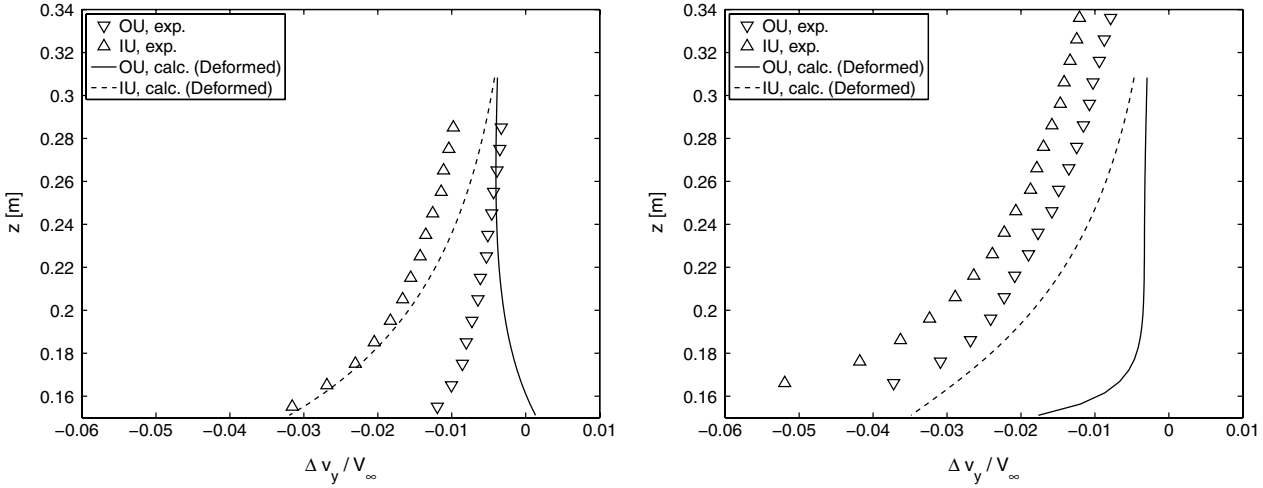


a) $\alpha = 0°$ b) $\alpha = 6°$

**Fig. 11 Nondimensional additional sidewash due to propeller installation, at the vertical tail plane, $T_c \approx 0.33$. Sidewash is defined positive in starboard direction.**

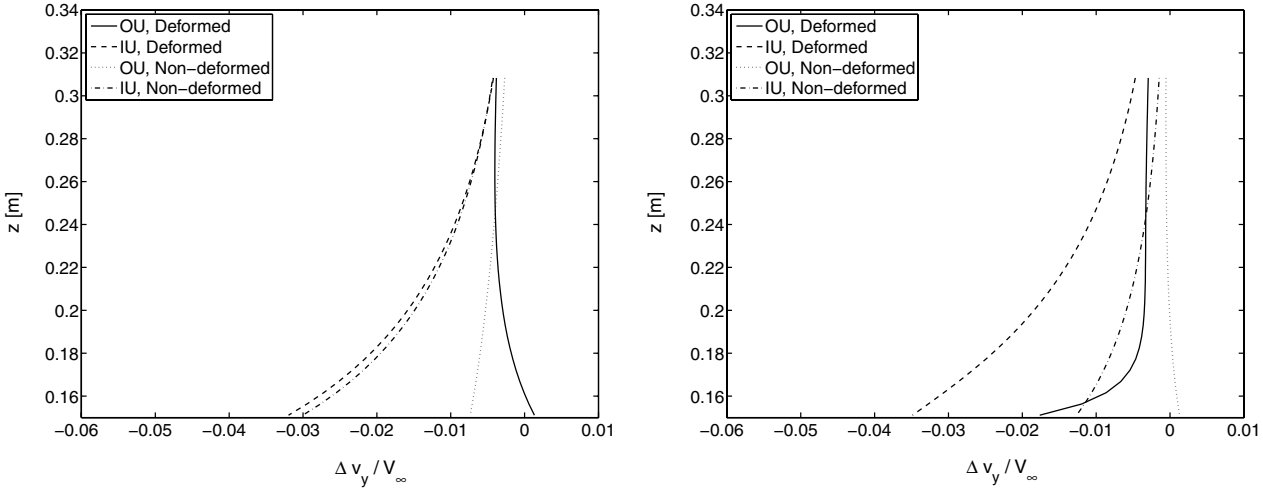


a) $\alpha = 0°$ b) $\alpha = 6°$

**Fig. 12 Effect of WTVS deformation on the sidewash at the vertical tail plane, $T_c \approx 0.33$.**

vortex has a major contribution to the sidewash at the vertical tail plane. Consequently, this vortex was tracked, in the measurements, along the fuselage at four stations as indicated in Figs. 3 and 5. Figures 13a and 13b show that the movement of the flap inner vortex for the working propeller side and the propeller inoperative side is small along the fuselage, for the most critical configuration. Comparing the measurement data to potential model results at both positions (Fig. 13b) a difference in flap inner vortex position can clearly be seen. Furthermore, there is a large unrealistic contribution of the inboard wing vortices impinging on the vertical tail. The resulting difference in crossflow is therefore probably caused by a discrepancy in lift distribution as well as an effect of dividing the continuous sheet into discrete elements. Subdividing the continuous vortex sheet into singular elements (trailing vortices) provides usable results as long as the positioning of the vortex elements is fixed, can be controlled or disturbances are small. In free wake models the approximation of a continuous vorticity sheet by discrete elements poses a problem when elements are close to each other (collocation points). To smoothen the singularities, viscous effects are included by applying a concrete viscous core [29]. These free wake models are only applicable if the distance between the point of interest and the vortex element is larger than 2 times the width of the original vortex element [19]. This condition is satisfied by the vertical tail plane, for the fuselage, on the other hand, this is not trivial. This observation is a likely cause for the discrepancy between the expected inner-flap tip vortex position from previous work [14,15] and currently measured.

The second effect is closely related to the lift distribution on the wing. This can be seen when comparing the sidewash measurements at zero- and six-deg angles of attack. Increasing the angle of attack increases the lift and, subsequently, the strength and asymmetry of the wing-lift distribution, resulting in a larger sidewash at the vertical tail. To investigate a potential difference in lift distribution between the measurements and potential-flow model, a simplified computational model has been implemented in the Fluent flow solver. This RANS model was compared with the configuration as measured by Mannée. Figure 14 shows an overestimation for both inboard and OU rotation, which might be caused by numerical diffusion in the rather coarse grid, which was chosen to limit the computing time. A possible resulting difference in vortical structure on both sides of the fuselage very likely leads to changes in the computed yawing moment coefficient. The trend of the yawing moment, on the other hand, is similar to the measured one, making it still useful for verification purposes.

The comparison of the lift distributions, as computed with the RANS and potential model, in Fig. 15a shows that the order of magnitude of the results is similar. The negligence of the swirl recovery due to the wing in the potential model, results in the overestimation of the total lift due to propeller rotation as seen in

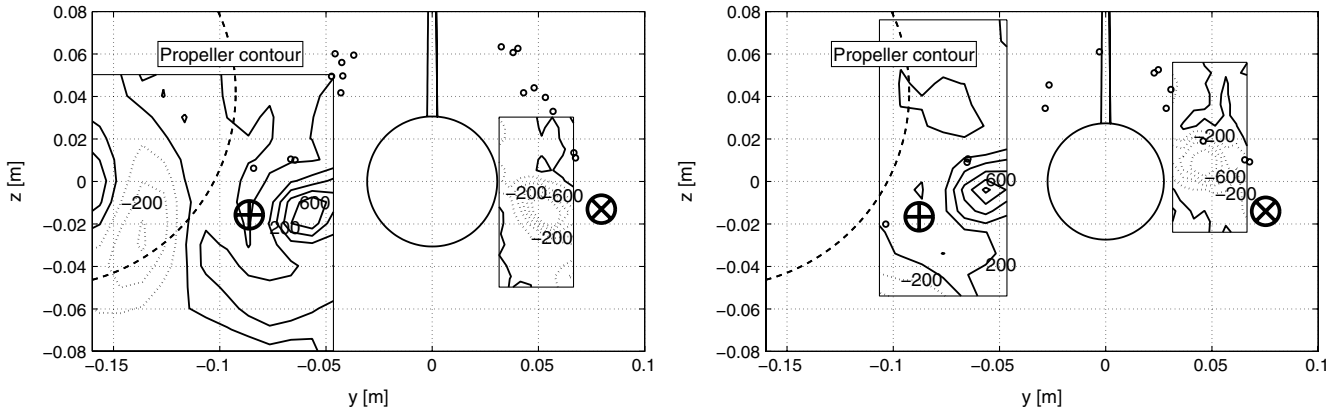


a) Station 1 b) Station 4

**Fig. 13 Measured flap inner vortex position as indicated by contours of constant axial vorticity, at $T_c \approx 0.33$, IU, $\alpha = 6°$, IU. \oplus, \otimes, and \circ are the calculated port and starboard inner-flap tip vortex and additional positions, respectively.**

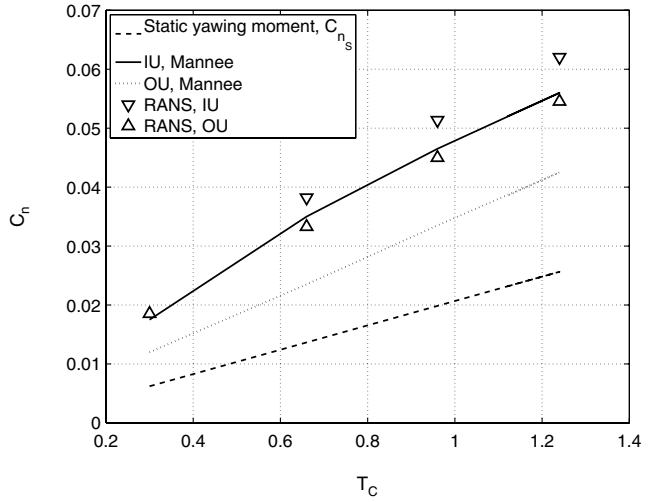


**Fig. 14 The yawing moment coefficient, measurements by Mannée and computations based on the combined RANS model; $\alpha = 5.8°$.**

Fig. 15. Nonetheless, the potential-flow method underestimates the wing lift while it overestimates the flap lift. The fact that the flap carries most of the additional load is due to the basic lifting line model (one vortex element over the wing and one over the flap) as shown in Fig. 15b. The additional overall load due to the flap deflection [14]

$$\frac{\partial \alpha}{\partial \delta} = \frac{3E}{2E+1} \tag{4}$$

is, however, comparable to the measurement results obtained by Schroijen and Slingerland [15] and Abbot and von Doenhoff [30]. $E$ is defined as the ratio between the flap chord and total (wing + flap) chord. The total wing lift with the contribution of the flap is therefore expected to be similar, and has been verified by adding more horseshoe vortices in chordwise direction. The chordwise distribution of load varied significantly whereas the total load remained fairly similar.

## IV. Conclusions

A first step towards a model supporting the sizing of the vertical tail of multiengine propeller aircraft has been created. The model calculates the forces and moments of the configuration with flaps deflected in OEI condition.

As was expected from the measurements performed by Mannée, the yawing moment coefficient with flaps deflected and OEI is significantly, approximately 1.5 times, larger than the static yawing moment (thrust times moment arm). The wind-tunnel measurements presented in this paper were performed with a thrust coefficient which is relatively small for takeoff conditions, however, the trend of the yawing moment increment due to the propeller slipstream interaction is clear. The most probable cause for this increment in yawing moment is the increased side force on the fin due to the

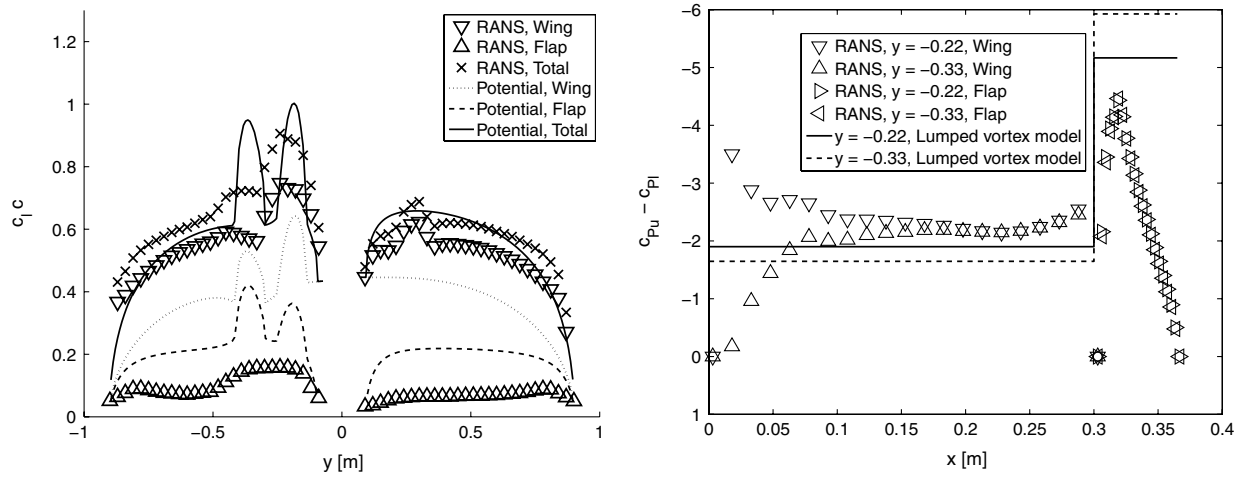


a) Lift distribution b) Chordwise pressure coefficient

**Fig. 15 Results of the RANS model and potential-flow method for the configuration as used by Mannée [31]; $\alpha = 5.8°$, $T_c = 1.3$, and propeller rotating IU.**

asymmetrical lift distribution over the wing/flap due to the propeller slipstream. This wing-lift distribution gives rise to an asymmetrical WTVS roll up which adds to the asymmetry of the flowfield. The asymmetric WTVS induces a sidewash at the fin location resulting in an additional contribution of the fin to the yawing moment.

The effects of the flap inner vortices on the fuselage were smaller than expected from previous numerical simulations, as were the displacements of the flap inner vortex due to the thrust setting. However the contribution of the asymmetry of the WTVS to the sidewash on the fin was underestimated. Therefore a more detailed study has to be performed on both the shape and strength of the WTVS.

Comparing the potential model results to the measurements it is found that the calculated yawing moment is generally underestimated. This is caused by a difference in lift distribution over the wing flap combination. This difference is most likely caused by neglecting wing thickness effects and propeller swirl reduction. The difference in lift distribution causes a difference in both strength and shape of the wing trailing vortex field. Adding to this are the flow singularities inherent in potential-flow modeling (vortex model). All these factors result in an underestimation of the sidewash at the fin and therefore an underestimation of the fin's contribution to the yawing moment. Creating a potential model for the design of the vertical tail should therefore include a detailed free wake model which is not influenced by the discontinuities inherent to potential models.

The results for the RANS simulation are encouraging with respect to the critical IU rotation case; the differences with measurement results are very likely to be caused by numerical dissipation due to a rather coarse grid. Additional computational fluid dynamics calculations using low dissipative schemes should be used to improve the computed results.

## References


[1] Torenbeek, E., *Synthesis of Subsonic Airplane Design*, 1st ed., Delft Univ. Press, Delft, The Netherlands, 1982, pp. 331–339.

[2] Raymer, D. P., *Aircraft Design: A Conceptual Approach*, 4th ed., AIAA Education Series, AIAA, Reston, VA, 2006, pp. 261–263.

[3] Mannée, J., "Windtunnel Investigation of the Influence of the Aircraft Configuration on the Yawing and Rolling Moments of a Twin-Engined Propeller Driven Aircraft with one Engine Inoperative," Nederlands Luchtvaart Lab. NLL A-1508 B, Amsterdam, 1962.

[4] Stuper, J., "Effect of Propeller Slipstream on Wing and Tail," NACA TM-0874, 1938.

[5] Veldhuis, L. L. M., "Propeller Wing Aerodynamic Interference," Ph.D. Thesis, Delft Univ. of Technology, Delft, The Netherlands, 2005.

[6] Gamble, B. J., and Reeder, M. F., "Experimental Analysis Of Propeller–Wing Interactions for a Micro Air Vehicle," *Journal of Aircraft*, Vol. 46, No. 1, 2009, pp. 65–73. doi:10.2514/1.34520

[7] Roosenboom, E. W. M., Heider, A., and Schroder, A., "Investigation of the Propeller Slipstream with Particle Image Velocimetry," *Journal of Aircraft*, Vol. 46, No. 2, 2009, pp. 442–449. doi:10.2514/1.33917

[8] Eshelby, M. E., "The Influence of Running Propellers on Low Speed Longitudinal Static Stability Trim Curves," Cranfield Inst. of Technology Aero Rept. 34, Cranfield, England, U.K., 1977.

[9] Katzoff, S., "Longitudinal Stability and Control with Special Reference to Slipstream Effects," NACA, R-690, 1940.

[10] Qin, E., Yang, G., and Li, F., "Numerical Analysis of the Interference Effect of Propeller Slipstream on Aircraft Flowfield," *Journal of Aircraft*, Vol. 35, No. 1, 1998, pp. 84–90. doi:10.2514/2.2263

[11] van Rooyen, R. S., and Eshelby, M. E., "Assessment of Propeller Influence on Lateral-Directional Stability of Multiengine Aircraft," *Journal of Aircraft*, Vol. 18, No. 5, 1981, pp. 364–371. doi:10.2514/3.44710

[12] van Nispen, A., "Slipstream Effects on the Static Lateral and Directional Control of a Multi-Engined Propeller Aircraft with One Engine Inoperative," M.Sc. Thesis, Delft Univ. of Technology, Delft, The Netherlands, 2002.

[13] van Nispen, A., and Slingerland, R., "Propeller Slipstream Effects on Lateral and Directional Controllability of Multi-Engined Aircraft," Society of Flight Test Engineers, Paper 33-26, Lancaster, CA, 2002.

[14] Schroijen, M. J. T., and Slingerland, R., "Propeller Slipstream Effects on Directional Aircraft Control with One Engine Inoperative," 45th AIAA Aerospace Sciences Meeting and Exhibit, AIAA Paper 2007-1046, 2007.

[15] Schroijen, M. J. T., and Slingerland, R., "Propeller Installation Effects on Multi-Engine Propeller Aircraft Directional Stability and Control," *Proceedings of the ICAS 2006 Congress*, Hamburg, Germany, 3–8 Sept. 2006, International Council of the Aeronautical Sciences, 6.10.2, 2006.

[16] Glauert, H., *The Elements of Aerofoil and Airscrew Theory*, 2nd ed., Cambridge Univ. Press, Cambridge, England, U.K., 1947, pp. 208–221.

[17] Durand, W. F. (ed.), *Aerodynamic Theory*, Vol. 4, Springer, Berlin, 1935, Chaps. K–N.

[18] Giesing, J. P., "Lifting Surface Theory for Wing–Fuselage Combinations,", Douglas Aircraft Co., DAC-67212, 1968.

[19] Katz, J., and Plotkin, A., *Low Speed Aerodynamics*, 2nd ed., Cambridge Univ. Press, Cambridge, England, U.K., 2001.

[20] Multhopp, H., "Aerodynamics of the Fuselage," NACA TM-1036, 1942.

[21] Betz, A., "Behavior of Vortex Systems," NACA TM-0713, 1932.

[22] Krasny, R., "Computation of Vortex Sheet Roll-Up in the Trefftz Plane," *Journal of Fluid Mechanics*, Vol. 184, 20 March 1987, pp. 123–155. doi:10.1017/S0022112087002830

[23] "Fluent 6.3 User's Guide," ANSYS, Inc., Lebanon, NH, 2006.

[24] Binkhorst, H., "Windtunnelmetingen aan een Model van de Fokker F-27 'Friendship' in de Lage-Snelheidstunnel van de Onderafdeling Vliegtuigbouwkunde," Technische Hogeschool Delft, M-47, Delft, The Netherlands, 1961.

[25] "Wing Body Yawing Moment and Sideforce Derivatives due to Sideslip: $N_v$ and $Y_v$ (with Addendum for Nacelle Effect)," Engineering Sciences Data Unit, Paper ESDU 79006, London, England, U.K., 2005.

[26] "Contribution of Fin to Sideforce, Yawing Moment and Rolling Moment Derivatives due to Sideslip, $(Y_v)_F$,$(N_v)_F$,$(L_v)_F$, in the Presence of Body, Wing and Tailplane," Engineering Sciences Data Unit, ESDU 82010, London, England, U.K., 2005

[27] Millicer, H. K., "Sidewash and Stability: A Study of Wing/Fuselage Interference Effects," *Flight*, Vol. 58, No. 2170, 27 July 1950, pp. 128–130.

[28] House, R. O., and Wallace, A. R., "Wind-Tunnel Investigation of Effect of Interference on Lateral-Stability Characteristics of Four NACA 23012 Wings, an Elliptical and a Circular Fuselage and Vertical Fins," NACA R-0705, 1941.

[29] von Timme, A., "Uber die Geschwindigkeitsverteilung in Wirbeln," *Archive of Applied Mechanics*, Vol. 25, No. 3, 1957, pp. 205–225. doi:10.1007/BF00536944

[30] Abbot, I. H., and von Doenhoff, A. E., *Theory of Wing Sections*, 2nd ed., Dover, New York, 1959, pp. 189–190.

[31] Mannée, J., "Windtunnel Onderzoek naar de Invloed van de Vliegtuigconfiguratie op Gier- en Rolmoment ten Gevolge van het Uitvallen van een Motor Bij een Tweemotorig Schroefvliegtuig," Nederlands Luchtvaart Lab., A-1508 A, Amsterdam, 1963.